RSC Advances

PAPER

View Article Online
View Journal | View Issue

Cite this: *RSC Adv.*, 2025, **15**, 3227

Exploring chiral and achiral properties of novel multilayer 3D polymers: synthesis and characterization†

Sai Zhang, *[a] Qingzheng Xu,[b] Xiuyuan Qin,[c] Yutin Wang,[a] Jialing Mao,[d] Yue Zhang[a] and Guigen Li *[e]

Received 10th January 2025
Accepted 27th January 2025

DOI: 10.1039/d5ra00233h

rsc.li/rsc-advances

This study reports the novel synthesis of multilayered 3D polymers *via* the 1,3,5-position coupling of 1,3,5-tris(4,4,5,5-tetramethyl-1,3,2-dioxaborolan-2-yl)benzene with 1,8-dibronaphthalene, a previously unreported method. The resulting polymers exhibit both achiral and chiral characteristics, offering a unique platform for structural and functional exploration. Comprehensive characterization using gel permeation chromatography, UV-vis spectroscopy, fluorescence measurements, circular dichroism, and scanning electron microscopy revealed intriguing optical properties and morphological features, promoting potential applications in photonics, sensors, and materials science.

Introduction

The development of advanced polymeric materials has garnered significant attention in recent years due to their versatile applications across various fields,[1] including optics,[2,3] electronics,[4] energy storage,[5,6] and material sensors.[7–12] Among these innovations, three-dimensional (3D) polymers have emerged as a particularly promising class of materials,[13–20] owing to their unique structural characteristics and enhanced properties compared to traditional two-dimensional polymers.[21,22] The ability to engineer the architecture of these materials at the molecular level allows for the manipulation of their physical, chemical, and optical properties, making them suitable for a wide range of applications.

One of the key strategies for synthesizing 3D polymers is using Suzuki coupling reactions,[23–25] which facilitate the formation of complex molecular architectures. The benzene 1,3,5-position coupling method has emerged as a promising strategy for creating multilayered polymer structures through the selective bonding of functionalized aromatic compounds. This approach facilitates the formation of robust networks with desirable mechanical and optical properties. However, its application in synthesizing multilayered 3D polymers remains underexplored, highlighting a gap in the existing literature.

Incorporating boron-containing compounds like 1,3,5-tris(4,4,5,5-tetramethyl-1,3,2-dioxaborolan-2-yl)benzene into polymer synthesis offers a novel strategy to enhance material properties. These boron-based building blocks facilitate versatile reactions, such as Suzuki coupling, enabling the creation of polymers with tailored optical activity and improved mechanical strength when combined with organic compounds like 1,8-dibromonaphthalene.

Optical activity, a phenomenon where certain materials exhibit the ability to rotate the plane of polarized light, is particularly significant in the context of chiral materials.[26–28] Chiral polymers have garnered considerable interest due to their potential applications in photonics,[29] where they can be utilized in devices such as optical switches, sensors, and displays. The capability to finely tune the chiral properties of polymers through sophisticated synthetic techniques paves the way for innovative designs in advanced optical materials. Furthermore, the exploration of circular dichroism (CD) spectroscopy empowers researchers to investigate the chiral characteristics of these materials, yielding critical insights into their structural organization and their interactions with light. This synergy between precise polymer synthesis and advanced spectroscopic analysis not only enhances our understanding of chiral materials but also opens transformative pathways for their application in emerging technologies.[30,31]

Characterization techniques are essential for elucidating the properties of newly synthesized polymers. Gel permeation chromatography (GPC) determines their molecular weight and

[a]*School of Pharmacy, Continuous Flow Engineering Laboratory of National Petroleum and Chemical Industry, Changzhou University, Changzhou, Jiangsu Province, 213164, China*

[b]*School of Chemistry and Chemical Engineering, Nanjing University, Nanjing, Jiangsu Province, 210093, China*

[c]*School of Life and Science, Nanjing Normal University, Nanjing, Jiangsu Province, 210046, China*

[d]*School of Environmental Science and Engineering, Continuous Flow Engineering Laboratory of National Petroleum and Chemical Industry, Changzhou University, Changzhou, Jiangsu Province, 213164, China*

[e]*Department of Chemistry and Biochemistry, Texas Tech University, Lubbock, Texas, 79415, USA*

† Electronic supplementary information (ESI) available. See DOI: https://doi.org/10.1039/d5ra00233h

polydispersity, while UV-vis spectroscopy and fluorescence assess optical behaviors. Additionally, polarization studies reveal anisotropic properties, and scanning electron microscopy (SEM) visualizes morphological features, connecting structure to function.

This study bridges a crucial gap in the existing literature by introducing a novel approach for synthesizing multilayered 3D polymers through a previously unreported 1,3,5-position coupling method. The resulting polymers possess a unique combination of achiral and chiral properties, providing an innovative platform for probing their structural and functional characteristics. Through a comprehensive suite of characterization techniques, we uncover compelling optical phenomena and distinctive morphological attributes that suggest exciting applications in photonics, sensors, and advanced materials science. This work not only enhances the current understanding of 3D polymer synthesis *via* innovative methodologies but also paves the way for the development of functional polymeric materials tailored for emerging technological applications.

Results and discussion

In the pursuit of synthesizing novel multilayered 3D polymer **3**, a retro-synthetic analysis[32] was conducted to evaluate potential synthetic routes. This analysis is crucial for identifying viable pathways that not only yield the desired polymeric structures but also consider the availability and accessibility of starting materials.

The first proposed synthetic route involves the use of 1,3,5-tris(4,4,5,5-tetramethyl-1,3,2-dioxaborolan-2-yl)benzene **2** and 1,8-dibromonaphthalene **1** as the key building blocks (Fig. 1). Notably, both of these starting materials are commercially available, which significantly enhances the practicality of this synthetic approach. The utilization of readily accessible precursors not only streamlines the synthesis process but also minimizes potential delays associated with sourcing specialized reagents. The 1,3,5-tris(4,4,5,5-tetramethyl-1,3,2-dioxaborolan-2-yl)benzene 2 serves as a versatile boron-containing compound that can participate in cross-coupling reactions, such as Suzuki coupling, with the electrophilic 1,8-dibromonaphthalene 1. This coupling reaction is anticipated to yield the desired multilayered 3D polymer with a well-defined architecture, thereby facilitating the exploration of its structural and functional properties. In contrast, the second proposed route considered the use of 1,3,5-tribromobenzene **2A** and 1,8-bis(4,4,5,5-tetramethyl-1,3,2-dioxaborolan-2-yl)naphthalene **1A** as the synthetic precursors. While this route presents an alternative pathway to achieve the targeted multilayer 3D polymer, it was ultimately deemed less favorable due to significant challenges associated with the synthesis of the latter starting material. The 1,8-bis(4,4,5,5-tetramethyl-1,3,2-dioxaborolan-2-yl)naphthalene **1A** is not commercially available and requires complex synthetic procedures that could involve multiple steps and low yields. The difficulties in procuring this precursor not only complicate the overall synthetic strategy but also introduce potential variability and inconsistencies in the synthesis. Consequently, the second route was abandoned in favor of the first, more straightforward approach. The decision to proceed with the first synthetic route is further supported by the advantages of employing commercially available reagents, which enhance the reproducibility and scalability of the synthesis. In addition, the use of established coupling methodologies, such as Suzuki coupling, allows for greater control over the reaction conditions and product formation.

The synthesis of polymers *via* 1,3,5-position coupling was successfully executed, leading to the formation of polymers **3**, **4**, **5**, and **6** (Fig. 2). The starting materials employed for the synthesis of polymers **3** and **4** were 1,3,5-tris(4,4,5,5-

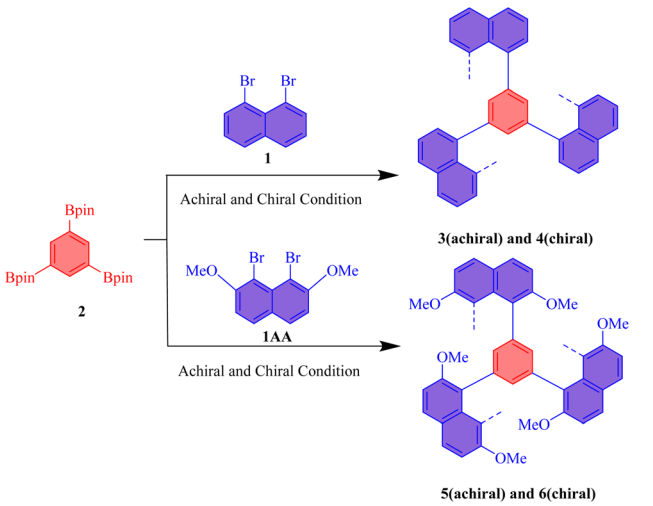

Fig. 2 Multilayer polymer **3–6**. All reactions were carried out with substrates **1**, **2**, **2A**, $Pd(PPh_3)_4$ or Pd[S-BINAP]Cl_2 and K_2CO_3 in THF/H_2O (10:2 mL) for 7 days under Ar.

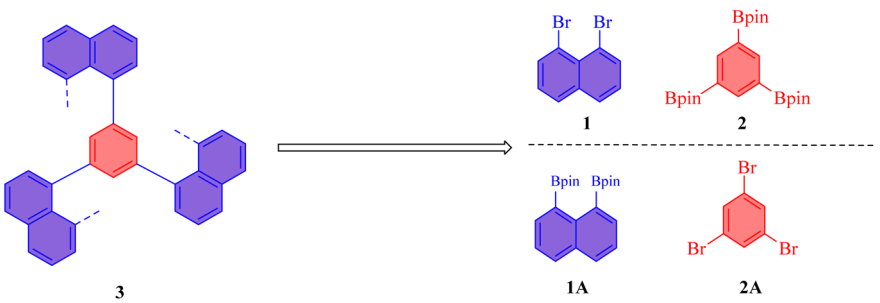

Fig. 1 Retro-synthetic analysis.

tetramethyl-1,3,2-dioxaborolan-2-yl)benzene **1** and 1,8-dibromonaphthalene **2** and 1,8-dibromo-2,7-dimethoxynaphthalene **1AA**. The polymerization reactions were conducted under both achiral and chiral conditions to investigate the influence of chirality on the molecular weight and polydispersity of the resulting polymers.

For polymers **3** and **4**, the characterization results under achiral conditions revealed a number-average molecular weight (M_n) of 9867 and a weight-average molecular weight (M_w) of 10 168, yielding a polydispersity index (PDI) of 1.030 (Table 1). These metrics indicate a relatively narrow molecular weight distribution, suggesting that the polymerization process proceeded with good control. In contrast, under chiral conditions, the polymers exhibited a decrease in molecular weights, with M_n recorded at 7325 and M_w at 7781, resulting in a PDI of 1.062. The observed reduction in molecular weight under chiral conditions may be attributed to the potential steric hindrance and altered reaction kinetics associated with the chiral environment. For polymers **5** and **6**, the characterization data under achiral conditions demonstrated M_w of 8183 and an M_n of 5520, leading to a PDI of 1.482 (Table 1). This higher polydispersity index suggests a broader distribution of molecular weights compared to polymers **3** and **4**, indicating a less controlled polymerization process. When subjected to chiral conditions, the polymers exhibited further decreases in molecular weights, with M_w decreasing to 5235 and M_n to 4153, resulting in a PDI of 1.261. The differences in molecular weight and polydispersity under varying conditions further underscore the influence of chirality on the polymerization process.

Table 1 Results of synthetic racemic polymer and oligomer

Poly-prod	Yield[a] (%)	M_w[b]	M_n[b]	PDI[c]	$[\alpha]_D^{20}$[d]
3	54	10 168	9867	1.030	—
4	35	7781	7325	1.062	−4 (c = 0.1)
5	35	8183	5520	1.482	—
6	41	5235	4153	1.261	−5 (c = 0.1)

[a] Isolated yield based on substrate **3–6**. [b] Determined by GPC with a polystyrene standard. [c] PDI = M_w/M_n. [d] In THF; c = g/100 mL.

The overall product yields for all synthesized polymers ranged between 35% and 54%, demonstrating reasonable efficiency in the coupling reactions. These yields indicate the successful formation of the target polymeric structures, while also reflecting the challenges inherent in achieving high yields in polymer synthesis. The optical rotation measurements under chiral conditions were recorded at −4° and −5° for polymers **3** and **4**, respectively. These negative optical rotation values suggest the presence of chirality within the polymer structures, which have implications for their optical properties and potential applications.

We investigated the optical properties of multilayer 3D polymers with both chiral and achiral architectures using UV-vis and photoluminescence (PL) spectroscopy (Fig. 3). The UV absorption spectra for both polymer types exhibited broad

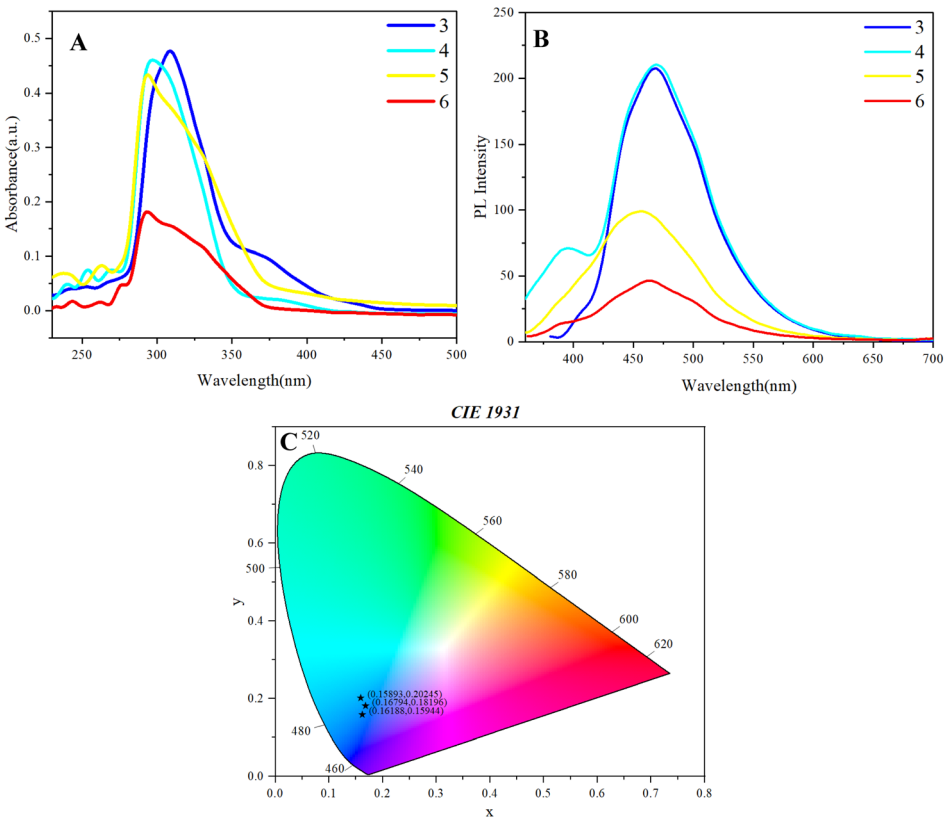

Fig. 3 (A) UV/vis absorption spectra of **3–6** in THF; c = 0.05 mg mL^{-1}. (B) PL spectra of **3–6** in THF; c = 0.05 mg mL^{-1}. (C) Coordinates 1931 chromaticity of polymer **3**, **5**, **6**.

peaks spanning the wavelength range of 270 nm to 450 nm, with the most pronounced absorption maxima located between 300 nm and 320 nm (Fig. 3A). Notably, all samples demonstrated a subtle tailing phenomenon beyond 375 nm, indicating the presence of extended π-conjugation or electronic transitions that contribute to the optical characteristics of these polymers. In the photoluminescence spectrum, the chiral polymer designated as polymer **4** exhibited a secondary peak at approximately 390 nm, which is indicative of specific electronic transitions associated with its chiral architecture (Fig. 3B). In contrast, the highest emission peaks for all polymer samples were consistently observed around 460 nm, suggesting a common luminescent behavior among the multilayer structures. The emission profiles exhibited a significant decay, with luminescence diminishing beyond 650 nm, which aligns with the expected behavior of such polymeric materials.

In the investigation of the CIE 1931 color coordinates for the synthesized multilayer 3D achiral and chiral polymers, a notable phenomenon of chromatic transfer was observed (Fig. 3C). Polymer **3** exhibited coordinates of (0.15893, 0.20245), while polymer **4**'s coordinates were nearly indistinguishable from those of polymer **3**, indicating a significant overlap in their chromatic properties despite potential differences in their molecular configurations. This similarity suggests that the structural characteristics inherent to these polymers may facilitate comparable light absorption and emission behaviors.

Conversely, polymers **5** and **6**, both of which incorporate methoxy substituents, displayed distinct color coordinates of (0.10794, 0.18196) and (0.16188, 0.15944), respectively. The presence of methoxy groups is known to alter the electronic distribution within the polymer chains, thereby influencing their optical properties and resulting in a divergence in colorimetric characteristics compared to polymers **3** and **4**. The multilayer 3D architecture of these polymers plays a crucial role in modulating their optical responses. The spatial arrangement of chromophores within the multilayer structure enhances light–matter interactions, potentially leading to phenomena such as energy transfer and exciton migration. These interactions can significantly impact the overall chromatic behavior of the materials, as evidenced by the varying coordinates. This study underscores the intricate relationship between molecular structure, multilayer configuration, and chromatic properties, providing valuable insights for the design of advanced polymeric materials in optoelectronic applications.

We investigated the aggregation-induced emission (AIE) phenomenon of multilayer 3D polymers through photoluminescence measurements in a solvent system comprising tetrahydrofuran (THF) and methanol (Fig. 4). The exploration of AIE behavior is particularly relevant for understanding the optical properties of these polymers, as it can influence their potential applications in optoelectronics and sensing technologies.[33]

For polymer **3**, which represents a multilayer 3D achiral architecture, the fluorescence intensity remained relatively stable across a methanol fraction range of 0% to 80% (Fig. 4A). This observation suggests that the polymer maintains its luminescent properties in mixed solvent environments up to this threshold. However, a notable quenching phenomenon was observed when the methanol fraction reached 90%. This quenching effect could be attributed to the increased polarity of the solvent mixture, which can lead to enhanced non-radiative decay processes and thereby diminish the fluorescence intensity. The stability of the fluorescence intensity at lower methanol fractions indicates that the polymer's structural integrity is preserved, allowing for efficient radiative transitions under these conditions. In the investigation of the multilayer 3D achiral polymer (polymer **4**), a notable phenomenon was observed wherein the introduction of methanol into the solvent system resulted in the emergence of new small peaks around 640 nm, in addition to the primary emission peak at 475 nm (Fig. 4B). This spectral evolution, particularly the subtle aggregation-induced emission (AIE) observed between 0% and 40% methanol, provides valuable insights into the polymer's photophysical properties.

The appearance of the 640 nm peaks can be attributed to the formation of excimer or exciplex states, which are commonly associated with intermolecular interactions in aggregated systems (Fig. 4B). As the methanol fraction increases, the polymer undergoes a transition from a solvated state to a more aggregated form. This aggregation restricts intramolecular motion, thereby reducing non-radiative decay pathways and enhancing the radiative transitions of excited states. Consequently, the emission spectrum exhibits red-shifted peaks characteristic of excimer formation, reflecting the lower energy transitions associated with these aggregated species. The subtle AIE phenomenon observed within the 0% to 40% methanol range indicates an optimal balance between solvation and aggregation, where partial aggregation promotes enhanced fluorescence. This behavior suggests that the polymer chains can achieve a conformation conducive to π–π stacking interactions, leading to increased luminescence efficiency. The initial increase in fluorescence intensity, coupled with the emergence of new emission peaks, underscores the complex interplay between solvent polarity and polymer conformation. The spectral changes observed in polymer **3** upon varying methanol fractions highlight the critical role of aggregation dynamics in modulating its fluorescence characteristics. The emergence of new peaks at longer wavelengths signifies the influence of excimer formation and supports the notion that AIE phenomena are intricately linked to the structural and electronic environment of the polymer in mixed solvent systems.

Furthermore, polymer **4**, a multilayer chiral 3D polymer, exhibited a different AIE behavior. The fluorescence intensity began to quench at methanol fractions between 0% and 50% (Fig. 4B), indicating a sensitivity to the solvent composition that is distinct from polymer **3** and polymer **4**. Notably, a partial AIE phenomenon was observed between 50% and 80% methanol, where the fluorescence intensity exhibited a temporary increase before undergoing further quenching at 90% methanol. This behavior suggests that the chiral architecture of polymer **5** could facilitate a unique interaction with the solvent that temporarily enhances its luminescence before the quenching effect dominates. The initial quenching at lower methanol

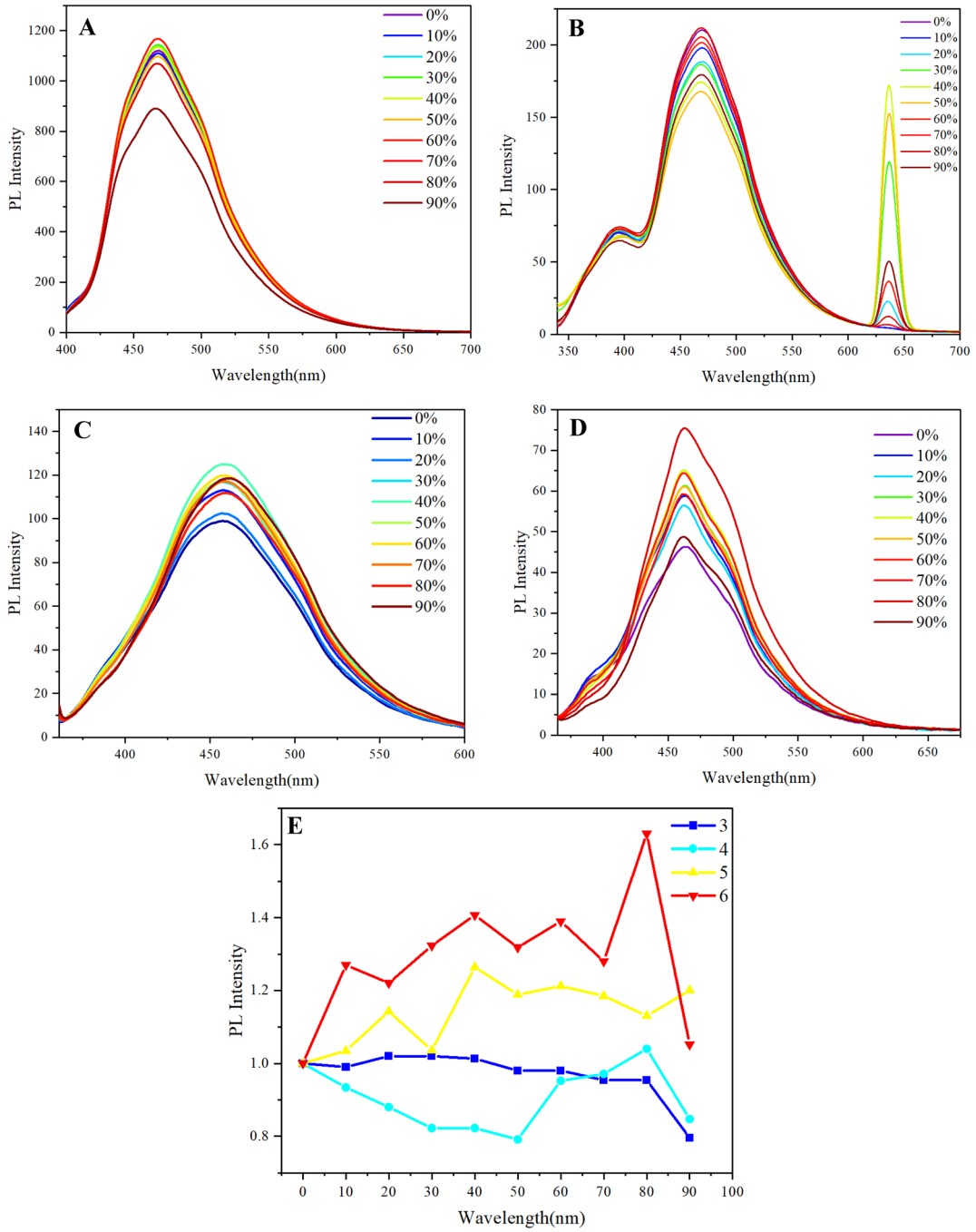

Fig. 4 (A)–(D) PL spectra of **3**, **4**, **5**, **6** in THF/methanol mixtures with different methanol fractions (f_w); $c = 0.05$ mg mL^{-1}; (E) Stern–Volmer plots of I/I_0 and methanol fraction.

fractions could be attributed to the disruption of the polymer's aggregate structure, which is essential for maintaining luminescence.

For polymer **5**, a multilayer 3D achiral polymer containing methoxy groups, the fluorescence intensity demonstrated an increasing trend with rising methanol fractions. Although this increase was not persistent, the fluorescence intensity remained higher than the initial level even at a methanol fraction of 90% (Fig. 4C). The presence of methoxy groups could play a crucial role in stabilizing the polymer's luminescence properties, potentially through intramolecular interactions that enhance radiative transitions. The gradual increase in fluorescence intensity suggests that the polymer may undergo structural changes that promote aggregation-induced emission, albeit with limitations at higher methanol concentrations.

Lastly, polymer **6**, a multilayer 3D chiral polymer, exhibited a pronounced AIE phenomenon when the methanol fraction ranged from 0% to 80% (Fig. 4D). Although a subtle decrease in fluorescence intensity was observed at 20% methanol, the overall AIE behavior remained acceptable and persistent

throughout this range. This observation highlights the robustness of the chiral polymer's luminescent properties, suggesting that its structural design effectively supports AIE even in varying solvent conditions. The persistence of the AIE phenomenon in polymer **6** indicates that the chiral architecture facilitates favorable interactions that enhance luminescence, contributing to the polymer's potential utility in applications requiring stable optical properties.

The Stern–Volmer plots associated with Fig. 4A–D illustrate the aggregation-induced emission (AIE) phenomenon, particularly observed in polymers **5** and **6** (Fig. 4E). Polymer **3** exhibits a decreasing trend in quenching, indicating a reduction in fluorescence intensity, while polymer **4** shows only subtle aggregation, as suggested by the minimal changes in fluorescence intensity with increasing water fraction.

The AIE behaviors observed across the different polymers underscore the significant influence of both chiral and achiral architectures, as well as the incorporation of functional groups, on their optical properties. The varying responses to methanol fractions reveal critical insights into the mechanisms governing fluorescence quenching and enhancement in these multilayer 3D polymers. These findings contribute to the broader understanding of AIE phenomena in polymeric materials and pave the way for the design of advanced materials with tailored optical properties for specific applications in optoelectronics and sensing technologies.

Subsequent investigations into the optical properties of 1,3,5-tri(naphthalen-1-yl)benzene **7** (the trimer) (Fig. 5A) revealed notable aggregation-induced emission (AIE) behaviour, particularly within a methanol fraction range of 0% to 50% (Fig. 5B and C). Within this range, the emission intensity of the trimer increased significantly as aggregation occurred, as demonstrated by the Stern–Volmer plot (Fig. 5D). Remarkably, even when the water fraction was increased to 90%, the intensity ratio (I/I_0) remained slightly elevated compared to its values at the initial water fractions of 0% and 10%. This observation suggests that the AIE characteristics of trimer **7** persist even under higher water fractions, indicating its potential stability and enhanced luminescence properties in various solvent environments.

Moreover, the UV-vis spectral characteristics of the trimer were found to closely resemble those of the synthesized multilayer 3D polymer (Fig. 5C), indicating a shared electronic environment and similar photophysical behavior. This correlation suggests that the structural features inherent to both the trimer and the multilayer polymer contribute to their optical responses, particularly in the context of AIE. These observations highlight the potential of multilayer 3D structures for designing

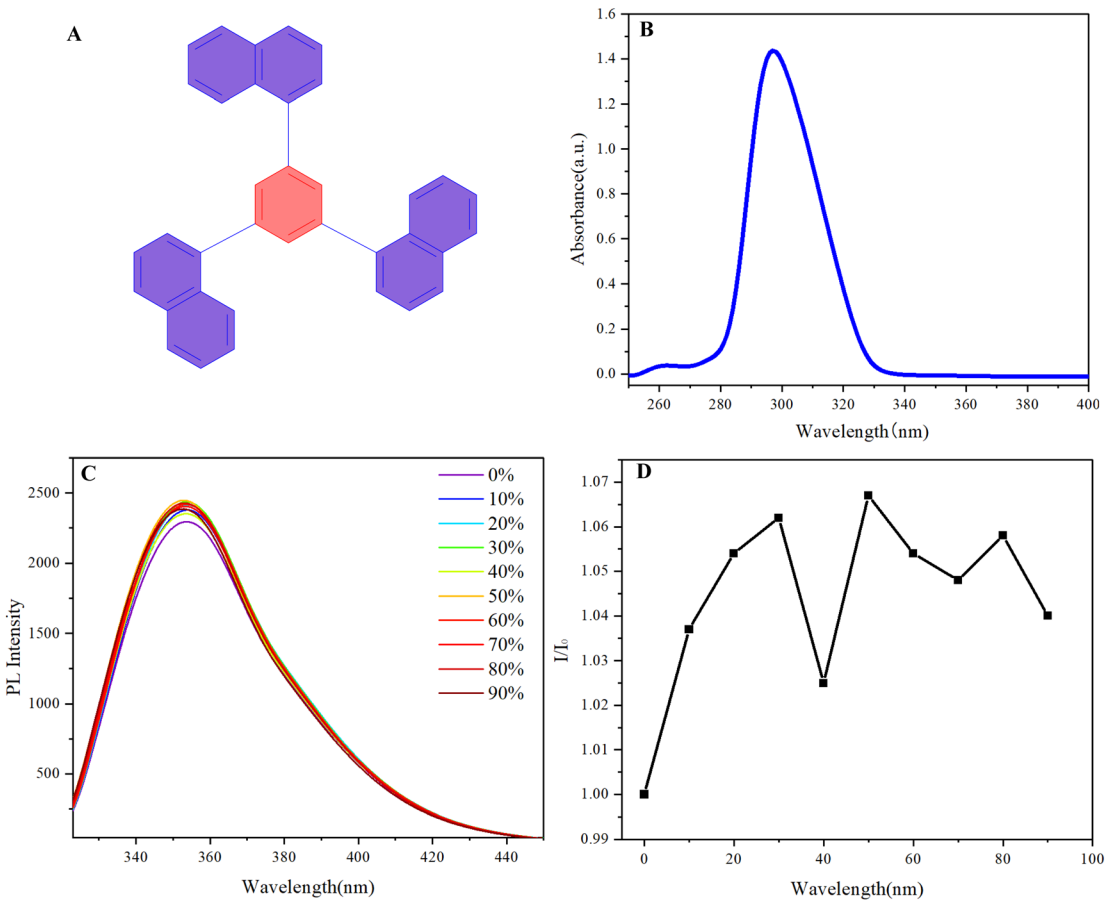

Fig. 5 (A). Compound **7** of trimer structure. (B). UV/vis absorption spectra of **7** in THF; $c = 0.05$ mg mL^{-1}. (C) PL spectra of compound **7** in THF/methanol mixtures with different methanol fractions (f_w); $c = 0.05$ mg mL^{-1}. (D) Stern–Volmer plots of I/I_0 and methanol fraction of compound **7**.

luminescent materials with tailored properties through careful manipulation of molecular architecture and aggregation behavior. The insights gained from these studies contribute to the broader understanding of AIE phenomena and their relevance in the development of advanced optoelectronic materials.

Dynamic light scattering (DLS) analysis was performed to investigate the particle size distribution of the synthetic achiral and chiral multilayer 3D polymers in a THF/methanol (50%/50%) solvent mixture. The achiral polymer exhibited prominent particle sizes corresponding to the highest percentage intensities at diameters of 272 nm and 496 nm (Fig. 6A and C). In contrast, the chiral polymer, which possesses a similar substructural framework, displayed peak particle sizes of 222 nm and 406 nm (Fig. 6B and D). These findings highlight a significant distinction in the aggregation behavior between the achiral and chiral multilayer 3D polymers. The larger particle sizes observed for the achiral polymer suggest a more effective aggregation process, likely driven by favorable intermolecular interactions that facilitate the formation of larger aggregates. This enhanced aggregation could be attributed to the absence of steric hindrance and the unrestricted packing of polymer chains, which are often advantageous in generating robust multilayer structures. Conversely, the smaller particle sizes of the chiral polymer indicate a less efficient aggregation process. The presence of chirality could introduce specific steric and electronic interactions that inhibit optimal packing and aggregation, leading to the formation of smaller aggregates. The reduced aggregation efficiency in the chiral multilayer 3D polymer could have implications for its structural integrity and functional properties, particularly in applications where larger, more stable aggregates are advantageous. Moreover, the characteristics of multilayer 3D chirality could further influence the material's properties, such as its optical behavior and mechanical strength. Chiral architecture can induce unique interactions among the layers, potentially affecting the overall stability and performance of the polymer. These chiral effects are crucial for the design and optimization of multilayer systems, as they can significantly impact the material's applicability in advanced technologies. The observed differences in particle size distribution between the achiral and chiral polymers underscore the critical role of chirality in influencing aggregation behavior within multilayer 3D structures.

Scanning electron microscopy (SEM) analysis of the synthetic chiral multilayer 3D polymer, synthesized *via* 1,3,5-position coupling, reveals distinct morphological differences between chiral and achiral systems (Fig. 7A–D). The SEM images

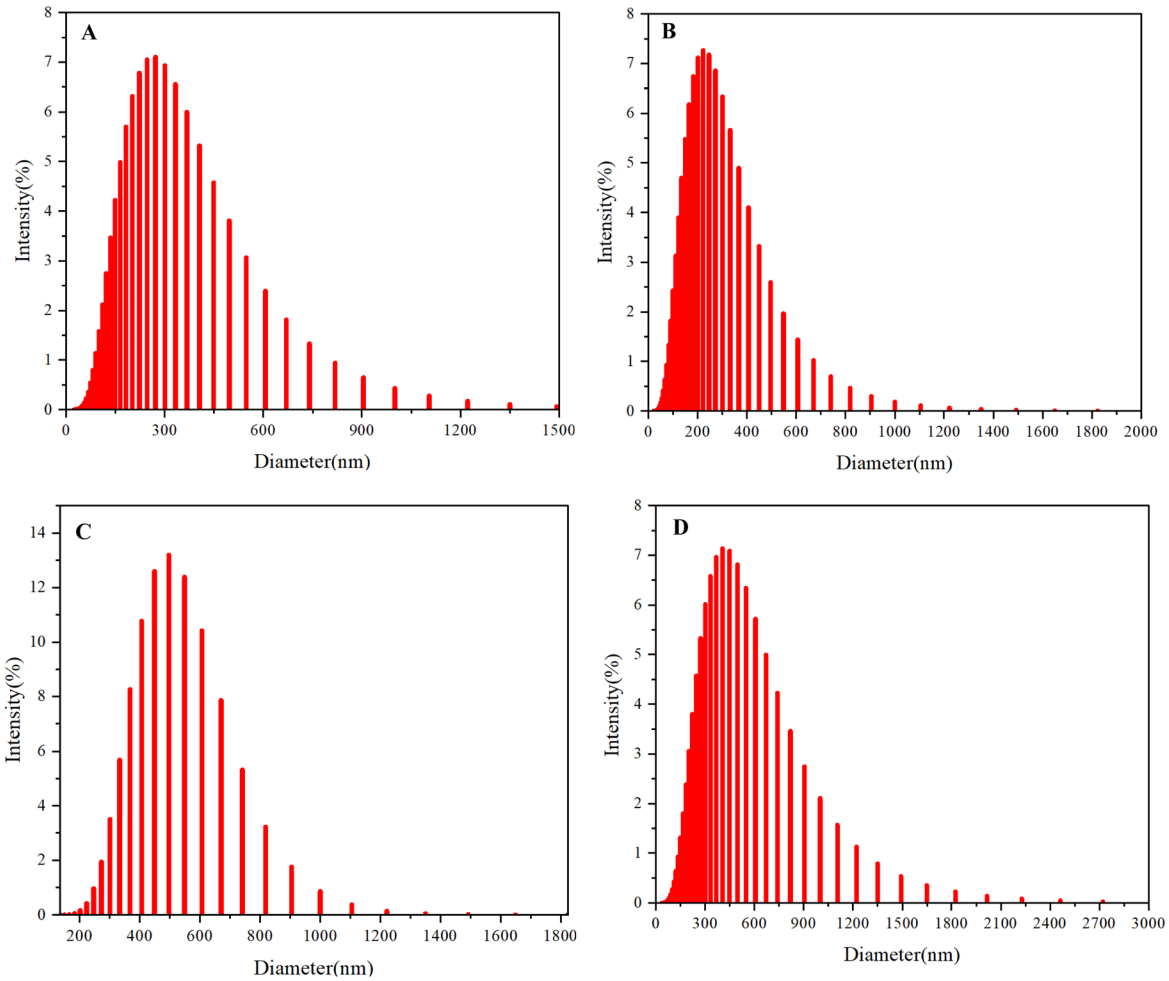

Fig. 6 (A–D) DLS particle size distribution of polymer **3–6** in THF/methanol mixture (50% : 50%).

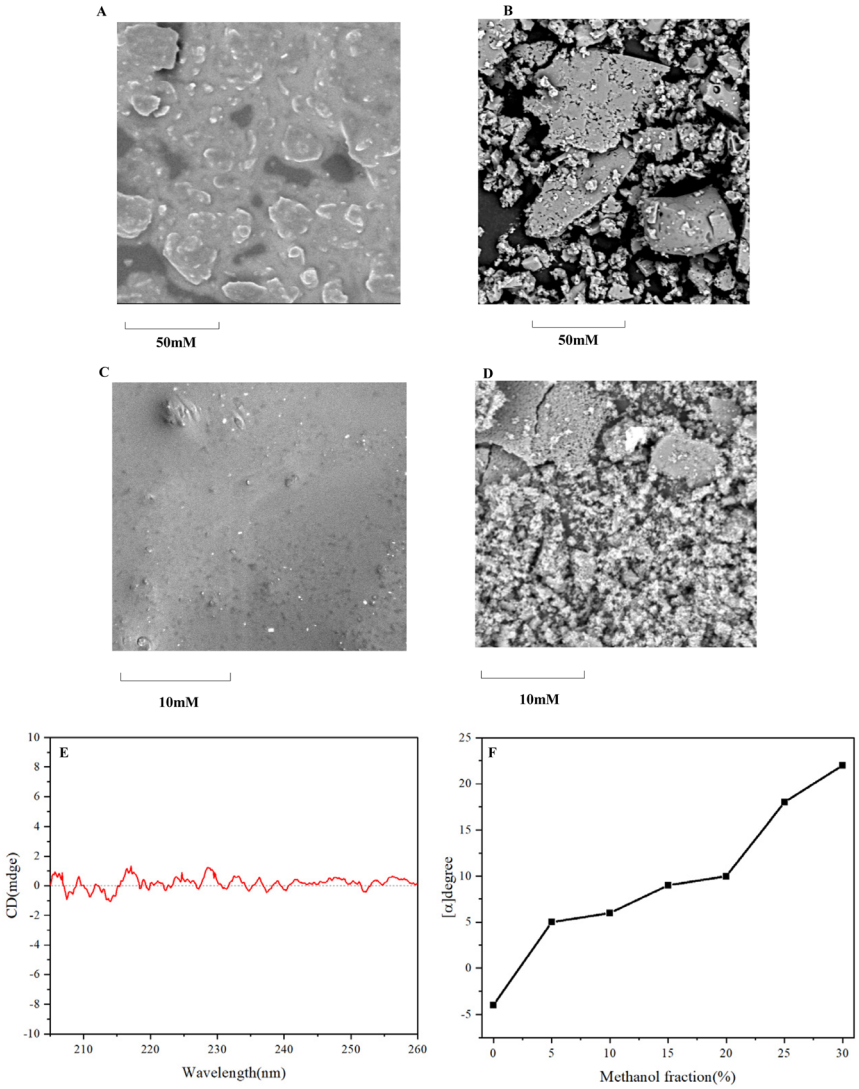

Fig. 7 (A) and (C) SEM picture of polymers **3** and **4**. (B) and (D) SEM picture of polymers **3** and **4**. (E) CD spectra of polymer **3** (0.02 mg in methanol). (F) Aggregation of induced polarization (AIP) of polymer **3** in THF and methanol mixture.

indicate that the achiral multilayer 3D polymers exhibit larger particle sizes compared to the chiral polymers. Notably, achiral polymers predominantly display a rock-like morphology, suggesting uniform aggregation, whereas chiral polymers demonstrate a mixed morphology of both rock-like and spherical particles. This variety in shape and size, supported by dynamic light scattering (DLS) measurements, reflects the asymmetric nature of chiral structures and highlights the role of chirality in influencing polymer aggregate size and morphology.

Circular dichroism (CD) spectroscopy was employed to investigate the chiroptical properties of the synthetic chiral multilayer 3D polymer **4** (Fig. 7E). The observed subtle Cotton effect within the wavelength range of −2 to 2 indicates the presence of chiral conformations within the polymer structure, albeit with limited intensity. This subtle signal suggests that the chiral arrangement of the polymer chains may lead to weak interactions that influence the electronic transitions of the chromophores embedded within the multilayer architecture. Furthermore, the aggregation-induced polarization (AIP) phenomenon was noted when the methanol fraction was varied between 0% and 25% (Fig. 7F). This observation implies that the solvent environment plays a critical role in modulating the aggregation behavior of the chiral multilayer 3D polymer. The increase in methanol content likely facilitates the formation of more defined aggregate structures, enhancing the chiral response and leading to observable polarization effects. These observations highlight the intricate relationship between solvent composition, polymer aggregation, and chiroptical properties in multilayer 3D chiral polymers. The ability to manipulate the chiral properties through solvent-induced aggregation presents potential avenues for optimizing these materials for applications in chiral sensing, catalysis, and optoelectronics.

Conclusions

In conclusion, this study successfully synthesizes multilayered 3D polymers through the novel 1,3,5-position coupling of 1,3,5-

tris(4,4,5,5-tetramethyl-1,3,2-dioxaborolan-2-yl)benzene and 1,8-dibronaphthalene—a previously unreported methodology. Characterization techniques, including GPC, UV-vis spectroscopy, CD spectroscopy, and SEM, reveal significant achiral and chiral properties, highlighting the polymers' potential applications in photonics, sensors, and materials science. This work enhances the understanding of 3D polymer synthesis through innovative coupling strategies and highlights the significance of chirality in influencing polymer properties. The insights gained from this research not only enhance the existing knowledge base but also pave the way for future investigations aimed at the development of oriental chirality,[34] turbo chirality,[35] and advanced functional polymeric materials tailored for specific applications.[36–40] Ultimately, this study underscores the potential of multilayered achiral and chiral polymers in driving innovation across multiple scientific disciplines.

Data availability

The data that support the findings of this study are available from the corresponding author upon reasonable request.

Author contributions

Sai Zhang: writing – original draft, data curation, methodology, investigation. Qingzheng Xu: writing – original draft, methodology, investigation. Xiuyuan Qin, Yuting Wang and Jialing Mao: investigation, data curation, methodology. Yue Zhang and Guigen Li: project administration and supervision. Sai Zhang, Qingzheng Xu, and Xiuyuan Qin contributed equally to this research.

Conflicts of interest

There are no conflicts to declare.

Acknowledgements

The authors acknowledge the financial support from the Robert A. Welch Foundation (D1361-20210327, USA), National Natural Science Foundation of China (22071102 and 91956110), and National Key Research Plan (2022YFC2105202).

References

1 Y. He, Y. Liu and M. Zhang, *Int. J. Biol. Macromol.*, 2024, **280**, 135657.
2 D. Thakur, Sushmita, S. A. Meena and A. K. Verma, *Chem. Rec.*, 2024, **24**, e202400058.
3 P. Chen, B.-Y. Wei, W. Hu and Y.-Q. Lu, *Adv. Mater.*, 2020, **32**, e1903665.
4 (*a*) T. C. Mokhena, M. J. Mochane, A. Mtibe, M. J. John, E. R. Sadiku and J. S. Sefadi, *Materials*, 2020, **13**, 934; (*b*) Z. Wang, J. Dai, J. Wang, X. Li, C. Pei, Y. Liu, J. Yan, L. Wang, S. Li, H. Li, X. Wang, X. Huang and W. Huang, *Research*, 2022, **2022**, 9767651.
5 T. Ji, X. Liu, H. Wang, Y. Shi, Y. Li, M. Zhang, J. Li, H. Liu and Z. X. Shen, *Research*, 2023, **2023**, 0092, DOI: **10.34133/research.0092**.
6 L. Shao, X. Lin, X. Yang, Y. Zhao, J. Zhang, T. Cheng and J. Zou, *Renew. Sustainable Energy Rev.*, 2025, **211**, 115332.
7 Y. He, X. Xu, S. Xiao, J. Wu, P. Zhou, L. Chen and H. Liu, *ACS Sens.*, 2024, **9**, 2275–2293.
8 Z. Fan, Z. Ji, F. Zhang, P. Luo, H. Zhang, J. Zhou, H. Cheng and Y. Ding, *Biomater. Sci.*, 2022, **10**, 4889–4901.
9 M. Jiang, J. Liao, C. Liu, J. Liu, P. Chen, J. Zhou, Z. Du, Y. Liu, Y. Luo, Y. Liu, F. Chen, X. Fang and X. Lin, *Front. Bioeng. Biotechnol.*, 2023, **11**, 1251713.
10 R. Qin, J. Nong, K. Wang, Y. Liu, S. Zhou, M. Hu, H. Zhao and G. Shan, *Adv. Mater.*, 2024, **36**, e2312761.
11 X. He, W. Ji, S. Xing, Z. Feng, H. Li, S. Lu, K. Du and X. Li, *Talanta*, 2024, **268**, 125283.
12 Q.-T. Lai, X.-H. Zhao, Q.-J. Sun, Z. Tang, X.-G. Tang and V. A. L. Roy, *Small*, 2023, **19**, e2300283.
13 G. Wu, Y. Liu, Z. Yang, L. Ma, Y. Tang, X. Zhao, H. Rouh, Q. Zheng, P. Zhou, J.-Y. Wang, F. Siddique, S. Zhang, S. Jin, D. Unruh, A. J. A. Aquino, H. Lischka, K. M. Hutchins and G. Li, *Research*, 2021, **2021**, 3565791.
14 J.-Y. Wang, Y. Tang, G.-Z. Wu, S. Zhang, H. Rouh, S. Jin, T. Xu, Y. Wang, D. Unruh, K. Surowiec, Y. Ma, Y. Li, C. Katz, H. Liang, W. Cong and G. Li, *Chem.–Eur. J.*, 2022, **28**, e202104102.
15 (*a*) Y. Tang, S. Jin, S. Zhang, G.-Z. Wu, J.-Y. Wang, T. Xu, Y. Wang, D. Unruh, K. Surowiec, Y. Ma, S. Wang, C. Katz, H. Liang, Y. Li, W. Cong and G. Li, *Research*, 2022, **2022**, 9847949; (*b*) Y. Tang, S. Zhang, T. Xu, Q. Yuan, J.-Y. Wang, S. Jin, Y. Wang, J. Pan, I. Griffin, D. Chen and G. Li, *Front. Chem.*, 2022, **10**, 962638, DOI: **10.3389/fchem.2022.962638**.
16 (*a*) S. Zhang, Q. Yuan and G. Li, *RSC Adv.*, 2024, **14**, 13342–13350; (*b*) S. Zhang, Q. Xu, X. Qin, J. Mao, Y. Zhang and G. Li, *Molecules*, 2024, **29**, 5641, DOI: **10.3390/molecules29235641**; (*c*) S. Zhang, Q. Xu, X. Qin, Q. Yuan, G. Li and Y. Zhang, *Macromol. Chem. Phys.*, 2024, 2400405, DOI: **10.1002/macp.202400405**.
17 (*a*) G. Dong, Z. Pan, B. Han, Y. Tao, X. Chen, G.-G. Luo, P. Sun, C. Sun and D. Sun, *Angew. Chem., Int. Ed. Engl.*, 2023, e202302595, DOI: **10.1002/anie.202302595**; (*b*) D. Zhu, Y. Zhu, Y. Chen, Q. Yan, H. Wu, C.-Y. Liu, X. Wang, L. B. Alemany, G. Gao, T. P. Senftle, Y. Peng, X. Wu and R. Verduzco, *Nat. Commun.*, 2865, DOI: **10.1038/s41467-023-38538-x**; (*c*) D. Zhu, Y. Chen, Y. Zhu, C.-Y. Liu, Q. Yan, X. Wu, K. Ling, X. Zhang, P. M. Ajayan, T. P. Senftle and R. Verduzco, *Macromolecules*, 2024, **57**, 1038–1049.
18 (*a*) C. Ai, Y. Zhang, S. Zhang and S. Yan, *ChemistrySelect*, 2024, **9**, e202402484, DOI: **10.1002/slct.202402484**; (*b*) S. Zhang, Q. Yuan, Q. Xu, S. Yan, Y. Zhang and G. Li, *RSC Adv.*, 2025, **15**, 2242–2249.
19 D. Lin, Y. Li, H. Zhang, S. Zhang, Y. Gao, T. Zhai, S. Hu, C. Sheng, H. Guo, C. Xu, Y. Wei, S. Li, Y. Han, Q. Feng, S. Wang, L. Xie and W. Huang, *Research*, 2023, **6**, 0027.

20 M.-L. Lin, M. Feng, J.-B. Wu, F.-R. Ran, T. Chen, W.-X. Luo, H. Wu, W.-P. Han, X. Zhang, X.-L. Liu, Y. Xu, H. Li, Y.-F. Wang and P.-H. Tan, *Research*, 2022, **2022**, 9819373.
21 H. Yu, D. T. L. Alexander, U. Aschauer and R. Häner, *Angew. Chem., Int. Ed. Engl.*, 2017, **56**, 5040–5044.
22 Z. Qin, Z. Li, S. Sharma, Y. Peng, R. Jin and G. Li, *Research*, 2022, **2022**, 0018.
23 A. Suzuki, *Angew. Chem., Int. Ed. Engl.*, 2011, **50**, 6722–6737.
24 A. Suzuki, *J. Organomet. Chem.*, 2002, **653**, 83–90.
25 D. Zhang and Q. Wang, *Coord. Chem. Rev.*, 2015, **286**, 1–16.
26 L. Ai, W. Xiang, Z.-W. Li, H. Liu, J. Xiao, H. Song, J. Yu, Z. Song, K. Zhu, Z. Pan, H. Wang and S. Lu, *Angew. Chem., Int. Ed. Engl.*, 2024, e202410988.
27 Z.-K. Zhu, T. Zhu, S. You, P. Yu, J. Wu, Y. Zeng, Y. Jiang, X. Liu, L. Li, C. Ji and J. Luo, *Adv. Sci.*, 2024, **11**, e2307593.
28 S.-Y. Xu, Q. Ma, Y. Gao, A. Kogar, A. Zong, A. M. Mier Valdivia, T. H. Dinh, S.-M. Huang, B. Singh, C.-H. Hsu, T.-R. Chang, J. P. C. Ruff, K. Watanabe, T. Taniguchi, H. Lin, G. Karapetrov, D. Xiao, P. Jarillo-Herrero and N. Gedik, *Nature*, 2020, **578**, 545–549.
29 L.-J. Chen, H.-B. Yang and M. Shionoya, *Chem. Soc. Rev.*, 2017, **46**, 2555–2576.
30 S. Li, X. Xu, C. A. Kocoj, C. Zhou, Y. Li, D. Chen, J. A. Bennett, S. Liu, L. Quan, S. Sarker, M. Liu, D. Y. Qiu and P. Guo, *Nat. Commun.*, 2024, **15**, 2573.
31 D. Okada and F. Araoka, *Angew. Chem., Int. Ed. Engl.*, 2024, **63**, e202402081.
32 (*a*) O. Piva, *Retrosynthetic Analysis and Synthesis of Natural Products 1: Synthetic Methods and Applications*, ISTE Ltd and John Wiley & Sons, London, England, 2019; (*b*) J. M. Smith, S. J. Harwood and P. S. Baran, *Acc. Chem. Res.*, 2018, **51**, 1807–1817.
33 B. Wang, Y. Liu, X. Chen, X.-T. Liu, Z. Liu and C. Lu, *Chem. Soc. Rev.*, 2024, **53**, 10189–10215.
34 S. Jin, Y. Wang, Y. Tang, J.-Y. Wang, T. Xu, J. Pan, S. Zhang, Q. Yuan, A. U. Rahman, J. D. McDonald, G.-Q. Wang, S. Li and G. Li, *Research*, 2022, **2022**, 0012.
35 T. Xu, Y. Wang, S. Jin, A. U. Rahman, X. Yan, Q. Yuan, H. Liu, J.-Y. Wang, W. Yan, Y. Jiao, R. Liang and G. Li, *Research*, 2024, **7**, 0474.
36 L. Cai, D. Xu, Z. Zhang, N. Li and Y. Zhao, *Research*, 2023, **6**, 0044.
37 M. W. Tibbitt, C. B. Rodell, J. A. Burdick and K. S. Anseth, *Proc. Natl. Acad. Sci. U. S. A.*, 2015, **112**, 14444–14451.
38 X. Zhang, G. Chen, L. Cai, L. Fan and Y. Zhao, *Research*, 2022, **2022**, 9797482.
39 (*a*) L. Chen, H. R. Low, Y. Jiang, W. Y. Zhang, C. K. Ao, Y. J. N. Tan, K. H. Lim and S. Soh, *Mater. Horiz.*, 2024, **11**, 1054–1064; (*b*) X. Ma, M. Zhou, L. Jia, G. Ling, J. Li, W. Huang and D. Wu, *Mater. Horiz.*, 2023, **10**, 107–121; (*c*) S. Wang, Y. Cao, Q. Peng, W. Huang and J. Wang, *Research*, 2023, **6**, 0112.
40 L. Luo, F. Zhang and J. Leng, *Research*, 2022, **2022**, 9767830.